 doi: 10.18287/JBPE23.09.020305

Side-by-Side OCE-Study of Elasticity and SHG-Characterization of Collagen Fibers in Breast Cancer Tissue before and after Chemotherapy

Anton A. Plekhanov[1*], Arseniy L. Potapov[1], Mikhail V. Pavlov[2], Vadim V. Elagin[1], Ekaterina V. Gubarkova[1], Alexander A. Sovetsky[3], Lev A. Matveev[3], Dmitriy A. Vorontsov[2], Alexander L. Matveyev[3], Alexey Y. Vorontsov[2], Sergey V. Gamayunov[2], Elena V. Zagaynova[1], Marina A. Sirotkina[1], Vladimir Y. Zaitsev[3†], and Natalia D. Gladkova[1†]

[1] Privolzhsky Research Medical University, 10/1 Minin and Pozharsky sq., Nizhny Novgorod 603950, Russia
[2] Nizhny Novgorod Regional Oncologic Hospital, 11/1 Delovaya str., Nizhny Novgorod 603093, Russia
[3] Institute of Applied Physics Russian Academy of Sciences, 46 Ulyanova str., Nizhny Novgorod 603950, Russia
[†] These authors contributed equally to this work

***e-mail:** strike_gor@mail.ru

Abstract. In the recent years promising results have been shown by the use of Compression optical coherence elastography (C-OCE) as a new optical biopsy approach to morphological assessment/diagnostics of human breast cancer using differences in elastic properties of morphological components of cancerous tissues. In this study, for the first time, a relationship was established between microstructural organization and biomechanical properties of breast-cancer tissue with pathomorphological changes caused by chemotherapy. To characterize texture of collagen fibers in the microenvironment of breast cancer, high-resolution visualization by Second-harmonic generation (SHG) microscopy was used. A side-by-side C-OCE and SHG imaging of patients' breast cancer tissues before and after chemotherapy was carried out. Regions of the cancer stroma (collagen fibers outside aggregates of cancer cells) were assessed separately from regions of cancer cell clusters penetrated by collagen fibers. For cancer stroma areas after chemotherapy, a statistically significant decrease in stiffness values was found. Simultaneously, parameters of collagen texture in SHG images (mean intensity, "coherency" and "energy") indicated increase in the collagen content, orientational orderliness, and collagen-texture heterogeneity. In contrast, cancer-cell areas post chemotherapy showed a statistically significant increase in stiffness. Analysis of SHG images of these regions indicated decrease in the inter-cellular collagen content and heterogeneity of its texture, whereas its orientational orderliness somewhat increased. The established negative correlation between stiffness and SHG parameters of collagen in cancer stroma indicates the contribution of the increase in orientational orderliness and total collagen content to the reduction in stiffness of breast cancer stroma after chemotherapy. For cancer-cell regions, significantly lower correlation between stiffness and SHG parameters (especially for coherency) was found, indicating stronger role of chemotherapy-induced changes in cancer cells themselves. These results give a deeper insight in the role of collagen texture organization in biomechanics of breast cancer tissues and contribute to a more detailed substantiation of the morphological characterization of breast cancer by C-OCE imaging.

Keywords: breast cancer; tissue stiffness; morphological assessment; compression optical coherence elastography (C-OCE); second-harmonic generation (SHG).

Paper #8959 received 20 Apr 2023; revised manuscript received 31 May 2023; accepted for publication 2 Jun 2023; published online 15 Jun 2023. doi: 10.18287/JBPE23.09.020305.

1 Introduction

Various optical technologies of bioimaging are being introduced into medical practice in the recent years, which has significantly extended possibilities for studying anatomical/structural features and functional state of patients [1]. In the last decade, a major progress was observed in the development of optical coherence tomography (OCT), where, in addition to unprecedented success of OCT usage in ophthalmic diagnostics, there was a significant advance in the abilities of OCT application for performing *in situ* optical biopsy enabling early cancer diagnosis and a deeper understanding of oncogenesis [2]. In addition to OCT-angiography that is already widely used in ophthalmology [3], other functional extensions of OCT technology are being tested for solving various clinical tasks. Such OCT modalities include, for example, cross-polarization OCT [4], OCT-lymphangiography [5], dynamic contrast OCT [6], or optical coherent elastography [7, 8]. In particular, the use of compression optical coherence elastography (C-OCE) makes it possible to distinguish morphological components of tissue based on mechanical contrast (e.g., in order to identify the location and boundaries of the pathology). Similarly, C-COE-based evaluation of biomechanical properties of morphological tissue components gives a deeper insight in biological mechanisms of the formation and course of a disease) [9]. The C-OCE technology has a resolution of 15–100 μm, which makes possible studying of biological tissue at the level of structural/morphological components or agglomeration of cells [10], which in many cases is quite sufficient, for example, for evaluation of the efficiency of cancer therapy [11, 12].

An important aspect of biomechanical visualization of functional changes occurring in tissues is evaluation and sufficiently ample understanding of contributions of various morphological components to the overall biomechanical properties of the tissue [13]. In this context, the use of C-OCE bodes well for studying biomechanical properties of tissue components in their natural state. During the last decade, C-OCE method has been attracting much attention in studies of elasticity of breast cancer tissues [8]. This is explained by high occurrence of breast cancer which is diagnosed in over 13% of women [14]. The use of C-OCE made it possible to establish characteristic elastic properties for various individual morphological components of breast cancer [15, 16], as well as for different morpho-molecular types of breast cancer [16–18] and formulate the corresponding C-OCE-based criteria of clean resection boundaries during breast-cancer surgery [19, 20]. C-OCE also made it possible to detect changes in elastic properties of cancer components (regions of cancer stroma and cancer cells themselves) after chemotherapy [11, 21]. In those studies, C-OCE revealed a paradoxical effect of increase in stiffness in regions of residual cancer cells after chemotherapy, whereas in histological images of these regions no obvious morphological changes were seen [22]. At the same time it is known that, for tumors demonstrating high resistance and weak response to therapy, specific structural changes are typical of extracellular matrix [23, 24] consisting mostly of type I collagen [25]. Besides, some connection was mentioned between the micro-environment of cancer cells, including specific organization of collagen bundles in cancer stroma, with early metastasis and occurrence of delayed recurrence [26, 27]. Those facts indicate the necessity of revealing the connection between the structure of collagen fibers and biomechanical properties of breast-cancer tissues in order to get a deeper insight in tumor evolution and better understanding of the morphological background of elastographic C-OCE images.

In this regard, in the present study we applied the second-harmonic generation (SHG) microscopy to visualize and quantitatively assess structure (texture) of collagen fibers in breast-cancer tissue before and after chemotherapy using excised tissue samples. Quantitative assessment of SHG images included evaluation of mean density of collagen (characterized by the mean intensity of SHG image), estimation of orientational ordering of collagen-fibers texture (using the parameter usually called “coherency”) and the parameter called “energy” to characterize the degree of heterogeneity of collagen texture. For the first time, we correlated the above-mentioned SHG-based characteristics of collagen-fibers texture in breast-cancer samples with the stiffness (Young’s modulus) of the same regions estimated using C-OCE. SHG microscopy allowed us to detect not only fairly thick collagen bundles (which were visible in histological images), but also isolated collagen fibers. Earlier studies indicated that SHG microscopy made it possible both qualitative and quantitative assessment of microenvironment of breast-cancer cells [28]. In this study we performed targeted analysis of morphologically different regions of cancer [29], namely, regions of cancer stroma sufficiently distant from agglomerates of cancer cells and regions of cancer cells themselves. For the regions of cancer stroma, characteristic range of stiffness was determined using C-OCE and parameters of collagen-fibers texture for these regions were estimated using SHG microscopy. For the regions of cancer cells,

we also determined the characteristic stiffness range using C-OCE, parameters of collagen texture using SHG microscopy. Besides, density of cancer cells was estimated for these regions using histological images.

The goal of this study was to reveal how the so-determined microstructural parameters and stiffness values for cancer stroma and cancer-cell agglomerates are related to pathomorphological changes in breast-cancer tissues caused by chemotherapy. Co-location of the same breast-cancer regions in the C-OCE and SHG-microscopy images made it possible to evaluate the complementary variations in stiffness and parameters of collagen fibers texture. The established correlation between the collagen texture parameters and biomechanical properties cancerous tissues gives a deeper insight in the morphological background of variations in stiffness of the main structural components of breast cancer after chemotherapy.

2 Materials and Methods

2.1 Patients and Therapy

The study complies with international and ethical standards set out in the World Medical Association Declaration of Helsinki "Ethical principles for medical research involving human subjects" [30]. The present study was approved by the Institutional Review Boards of the Nizhny Novgorod Regional Oncologic Hospital (protocol #12 of December 23, 2021). All patients included in the study provided written informed consent prior to enrolment. The patients (the mean age is 62 years; age range 34–76 years) were treated in the Nizhny Novgorod Regional Oncologic Hospital in 2018–2022 and had been morphologically diagnosed with locally advanced breast cancers ($T_{2\text{-}3}N_{0\text{-}1}M_0$ stages). Patients were prescribed courses of neoadjuvant chemotherapy according to the clinical guidelines [31], consisting of 4 cycles of AC (Adriamycin & Cytoxan) given at 3 weekly intervals comprising doxorubicin (60 mg/m^2) and cyclophosphamide (600 mg/m^2), all given by intravenous injection followed by 12 weekly paclitaxel (80 mg/m^2) injections. Following completion of primary chemotherapy before surgical resection, assessments of the responses and tumor bed detection were performed clinically by ultrasound. The surgical procedure (total mastectomy) was carried out between the 2nd and 6th weeks following the completion of chemotherapy. All patients had histologically proven invasive adenocarcinoma (Luminal-B Her2 negative (n = 3) and Triple-negative (n = 7) subtypes) without detectable metastatic disease prior to commencing chemotherapy.

2.2 Study Design

Breast cancer tissues of 10 patients obtained by core needle biopsy (before chemotherapy) and surgical resection (after completion of chemotherapy) were examined (Figs. 1A–B). Two fresh tissue samples per patient were obtained, a core-needle biopsy tissue sample (~1.5 × 0.1 × 0.1 cm) and surgically excised tissue samples (~3.0 × 1.0 × 0.5 cm). Breast cancer tissue samples were delivered within one hour after punctation/resection to the laboratory in 10% solution of bovine serum albumin on ice. At the first stage, C-OCE studies of fresh breast cancer tissues were carried out for 20–25 min (Fig. 1C). During C-OCE visualization, we used a 3D positioning system [32], which enabled both high-precision positioning of the probe in lateral directions (with an accuracy of 10 μm), as well vertical movement of the probe required for performing controlled compression of the studied tissue samples. Immediately after the C-OCE study, samples were subjected to histological preparation (Fig. 1D). At the second stage, a histological examination of the prepared histological slides was carried out for targeted comparison with C-OCE images to evaluate the cancer response to chemotherapy, as well as to assess the cancer-cell density in pre- and post-chemotherapy samples (Fig. 1E). To analyze the organization of collagen fibers, deparaffinized unstained histological sections were studied using SHG microscopy (Fig. 1F).

For subsequent quantitative assessment of cell density (in histological images), stiffness values (in C-OCE images) and collagen fibers texture parameters (in SHG images), two types of breast cancer tissue areas before/after chemotherapy were analyzed: cancer stroma (collagen fibers in the projection of the anatomical tumor bed, but outside cancer-cell regions) and cancer-cell regions themselves (clusters of cancer cells and penetrating collagen fibers in the tumor bulk) (Figs. 1G–I).

2.3 Compression Optical Coherence Elastography (C-OCE)

A custom-made spectral-domain multimodal OCT device (Institute of Applied Physics of Russian Academy of Sciences, Russia) was used [33]. The OCT device had the following characteristics: a central wavelength of 1.3 μm, spectral width of 90 nm, spectral-fringe rate of 20 kHz, radiation power on the sample of 2 mW, axial resolution of 10 μm, lateral resolution of 15 μm, and scanning depth of 2 mm in air.

For characterization of tissue elasticity we use the variant of quantitative C-OCE described in detail in previous works [34–38]. In this C-OCE method, a thin layer of translucent silicone with pre-calibrated Young's modulus is placed onto the surface of the studied tissue. This sandwich structure silicone-tissue is slightly compressed by the output window of the OCT probe and a series of complex-valued OCT scans is acquired during this process. In the course of compression, the tissue and silicone are allowed to freely expand laterally, so that their elastic response is determined by the Young's moduli of the silicone and tissue. It was carefully verified that silicone is a highly elastically linear material, so that its cumulative strain is proportional to the elastic stress applied to the compressed sandwich structure. Consequently, by plotting the cumulative strain in the

silicone against the strain in the tissue beneath one obtains stress-strain curves $\sigma(\varepsilon)$ characterizing the tissue elasticity [37]. These stress-strain curves are pronouncedly nonlinear for the majority of real tissues, so that the local slope $d\sigma / d\varepsilon = E_{tg}$ of such a curve yields the tangent Young's modulus E_{tg} of the tissue. In was shown in previous studies [11, 16, 17, 39] that the tangent Young's modulus in breast-cancer tissue is pronouncedly stress-dependent and may vary several times and even more when the applied stress varies in the range of several kPa. In view of this, for reliable quantitative conclusions, reproducibility and comparison of different measurements, the Young's modulus (stiffness) of the tissue should be estimated for the same pre-chosen stress level [37]. It was experimentally verified that a stress level of 4 kPa is quite a convenient value for measurement procedures and at the same time different morphological components of breast-cancer tissue often demonstrate better contrast in their stiffness than for significantly higher and significantly lower stress [16, 37].

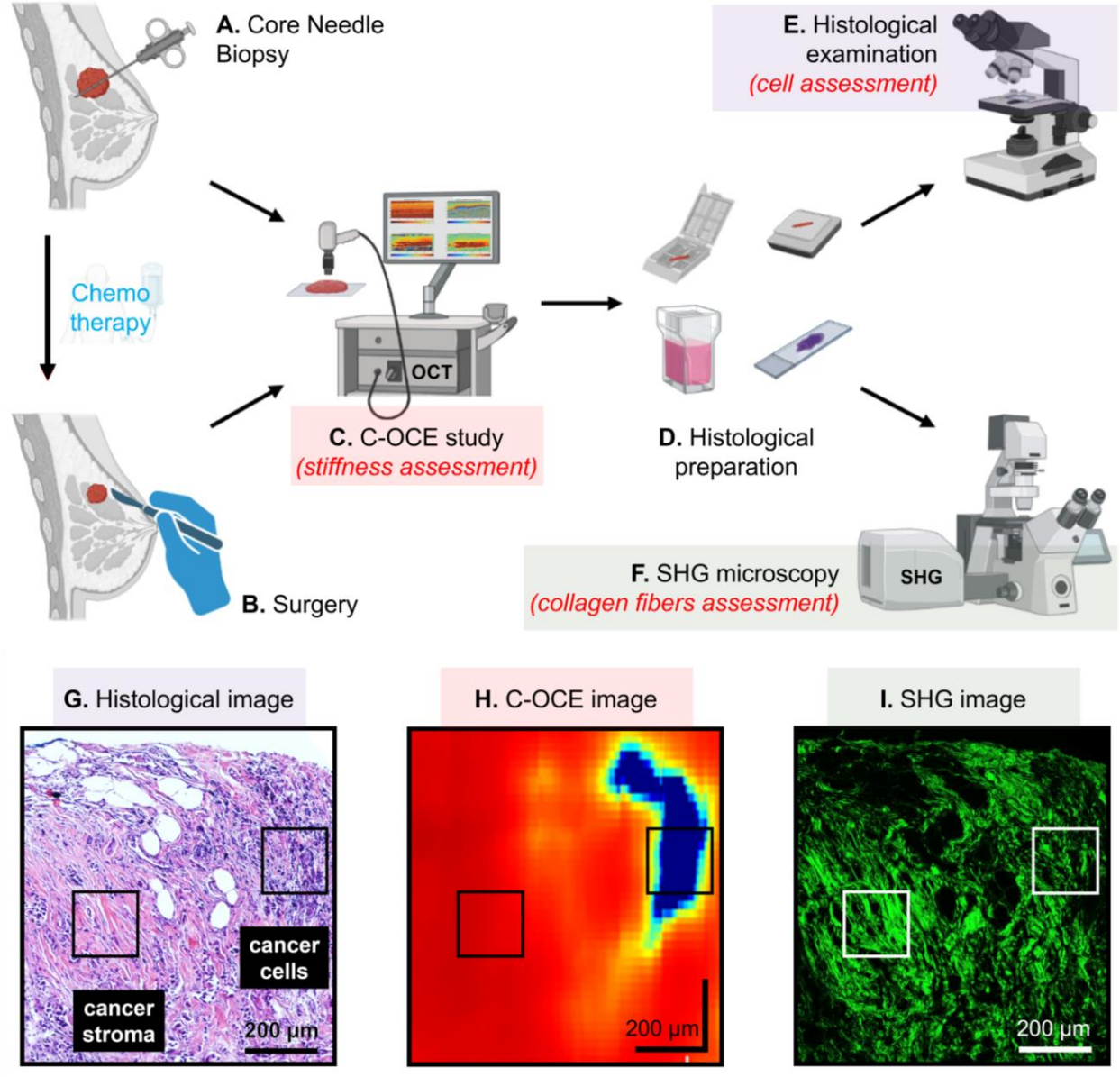

Fig. 1 Schematic of the study design demonstrating all main steps with representative images of various types. (A) harvesting of core needle biopsy samples before chemotherapy and (B) surgical excision of cancer samples after chemotherapy. (C) C-OCE examination of the fresh-tissue followed by histological preparation (D). (E) morphological assessment of the cancer-cell component; (F) SHG-based assessment of collagen fibers texture parameters; representative co-located histological image (G), C-OCE-based stiffness map (H) and SHG image (I). The images demonstrate the possibility of gathering various-type data for the same tissue regions for subsequent quantitative assessment of the corresponding parameters within a standard-size ROI of 180 × 180 μm in size. Two of such ROI are shown in panels (G), (H), and (I) by rectanges, one corresponding to cancer stroma and the other to a cancer cell region.

This fact is important for detection of tumor zones, for which the maximal contrast between the cancer cell areas with high stiffness values and stroma areas with medium/low stiffness values is usually observed at an intermediate (neither very low, no too high) stress level about a few kPa [16]. In this study, we adopted the "standardized" stress level ~ 4kPa. For this stress, it was previously established in Ref. [17] and confirmed in several independent studied [16, 18, 21, 40] on the possibility to differentiate stiffer breast cancer cell areas from the surrounding softer stroma areas that a stiffness of 420 kPa can be taken as the boundary (threshold) value. This conclusion is also true for breast cancer tissue after chemotherapy [21, 22].

2.4 Second-Harmonic Generation (SHG) Microscopy

In this study, we use SHG microscopy as a high-resolution method for visualizing type I collagen fibers, which play a major structural role in the tumorous stroma. The study was carried out on deparaffinized unstained sections 7 μm thick, which were made together with strained sections for histological examination. This allowed identical structures to be observed on both SHG images (Fig. 1I) and histological images (Fig. 1G).

A multiphoton laser scanning microscope LSM 880 (Carl Zeiss, Germany) was used. The images were constructed using an objective with a "C Plan-Apochromat" ×40/1.3 NA oil immersion, the field of view is 212 × 212 μm (image size 1024 × 1024 px). The source of the exciting radiation was Ti:Sapphire femtosecond laser Mai Tai HP (Spectra Physics, USA). The excitation wavelength was 800 nm. The average laser power was maintained at 3 mW. The SHG signal was detected using spectral selection in the wavelength range 370 to 420 nm. The images were detected from the back-scattered SHG signal.

2.5 Histological Examination

Immediately after C-OCE study, for co-location, the positions of the C-OCE scans were marked on the surface of the studied samples using the histological ink (Histo-Line, blue). Samples were fixed in 10% formalin for 48 h and then dehydrated using a gradient ethanol bath, followed by xylene purification and paraffin embedding. Then several (3–6) serial sections with a thickness of 7 μm were made along the direction coinciding with the C-OCE-scan position. Histological sections were stained according to the standard technique with hematoxylin and eosin (H & E), which made it possible to assess the breast cancer tissue structures (cancer cells and stroma) and to carry out an accurately comparison of histological and C-OCE images (Figs. 1G–H), which is described in detail in the papers [11, 17].

According to the results of histological examination, among the ten studied cases of breast cancer, only two showed a pathological complete response to neoadjuvant chemotherapy, which was expressed in the absence of residual cancer cells. For eight other cases, cancer cells areas were identified and analyzed both before and after chemotherapy. Cancer stroma areas were analyzed for all ten cases of breast cancer before and after chemotherapy.

2.6 Quantification of the Examination Results

We emphasize once again that quantitative assessment of histological, C-OCE and SHG images was made for the two types of breast cancer tissue areas, i.e., before and after chemotherapy. We analyzed separately the cancer stroma (collagen fibers in the projection of the anatomical tumor bed, but away from cancer cells) and cancer cells (clusters of cancer cells and collagen fibers in tumor bulk) (Fig. 1G). To analyze the cellular density by histological images of breast cancer, the number of cancer cell nuclei in a region of interest (ROI) of 180 μm^2 was counted (squares in Fig. 1G) and calculated using the multipoint tool in ImageJ 1.8.0 software (NIH, USA). The same size of areas (for cancer stroma and cancer cells) was used for quantitative analysis of parameters in C-OCE and SHG images (Figs. 1H–I). For the statistical calculation of parameters, 30 areas of the cancer stroma and 30 areas of cancer cells (with the exception of two cases of pathologically complete response) were analyzed for each patients' breast cancer tissue both before and after chemotherapy.

As mentioned in Section 2.3, for quantitative assessment of C-OCE data, the analyzed elastographic maps correspond to the stress-standardization level of 4 kPa. The "local" stiffness was estimated as a mean value over a rectangular ROI with a side size 180 μm^2.

In order to quantify the state of type I collagen fibers in the studied ROIs, the methods of first-order statistics (mean signal intensity) and texture analysis (coherency, energy) of SHG images were applied. These methods are able to quantify changes in collagen fibers texture caused by various pathological conditions [41] and are widely used in SHG image analysis [42]. The average intensity of the SHG signal reflects the relative amount of collagen fibers in the ROI [43]. Coherency is directly proportional to the degree of ordering of the packaging of collagen fibers and reflects the degree of alignment (the existence dominant direction) of the fibers [44]. The "energy" parameter characterizes the degree of the texture heterogeneity. High energy values occur when the gray level distribution is characterized by high spatial gradients. In our case, this corresponds to a highly heterogeneous texture of collagen fibers in the ROI. The mean intensity of SHG-signal was calculated using ImageJ's histogram analysis toolbox [45] and "coherency" and "energy" parameters of the SHG-visualized collagen texture were calculated using the OrientationJ plugin [46] (see Appendix section for a more detailed information).

2.7 Statistics

The variable for statistical intergroup (before/after chemotherapy) comparison was the average stiffness (elastic Young's modulus) calculated from the C-OCE images, as well as the indices of the subsequent tissue morphological measuring (cell density, mean signal

intensity, coherency, and energy of collagen fibers) for tissue areas of cancer stroma and cancer cells. For quantitative comparative analysis of these parameters all results are expressed as mean ± SD. Box plots were used for graphical presentation of data and indicate the median, lower/upper quartiles (25th and 75th percentile), and 5th and 95th percentile. The non-parametric Wilcoxon signed-rank test is a were used to detect significant differences in numerical data between related studied groups (from patient before/after chemotherapy). The results were considered statistically significant if the p value was < 0.05. The Spearman's correlation coefficient (r) was calculated to determine the correlation between stiffness values according to the C-OCE data and mean signal intensity, coherency, and energy parameters of collagen fibers according to SHG data or cancer cell density according to histology data.

The calculations were carried out using the GraphPad Prism 8.0 (San Diego, CA, USA) and the Statistical Package for Social Sciences 26.0 (Chicago, IL, USA).

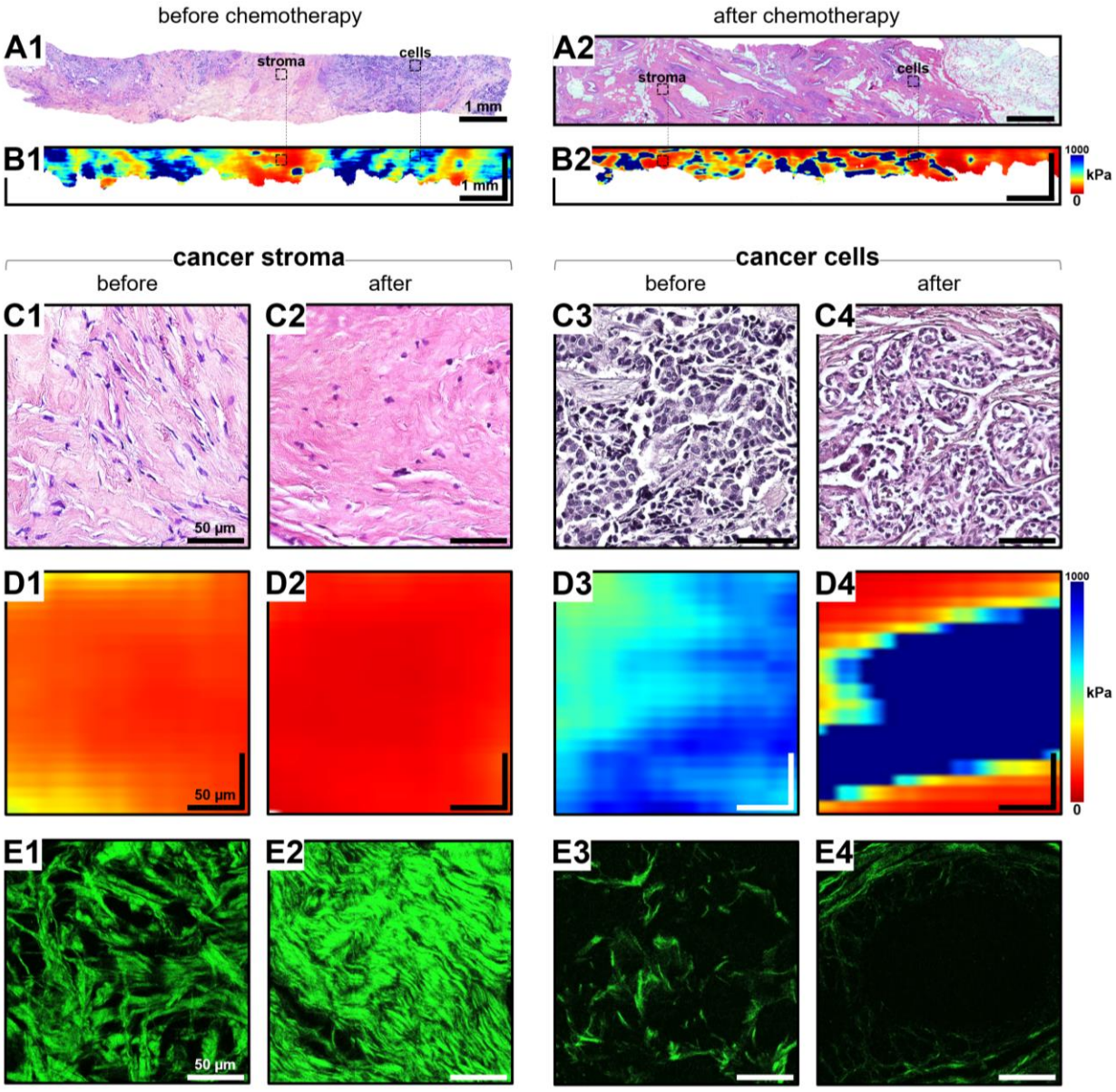

Fig. 2 Representative examples of various images obtained for breast-cancer samples from one patient. Characteristic histological images (A) and C-OCE-based stiffness maps (B) obtained before (A1–B1) and after (A2–B2) chemotherapy. Panels (C)–(E) demonstrate zoomed histological images (C), C-OCE-based stiffness maps (D) and SHG-microscopy images (E) for the analyzed regions of cancer stroma and cancer cells before and after chemotherapy. For cancer stroma images, clear reduction in stiffness is visible in C-OCE images (see D1 and D2), whereas SHG images (E1–E2) demonstrate increase in the collagen content (via increase in the SHG-signal intensity), increase in the orientational ordering (i.e., increase in the coherency parameter) and increase in spatial heterogeneity (expressed via energy parameter of the collagen fibers texture) after chemotherapy. For cancer-cell regions, in contrast to stroma, stiffness increases (D3–D4), collagen content decreases after chemotheraphy. The trends for the coherency and energy of the collagen fibers texture are not visually evident and results of their quantification are shown in Fig. 3.

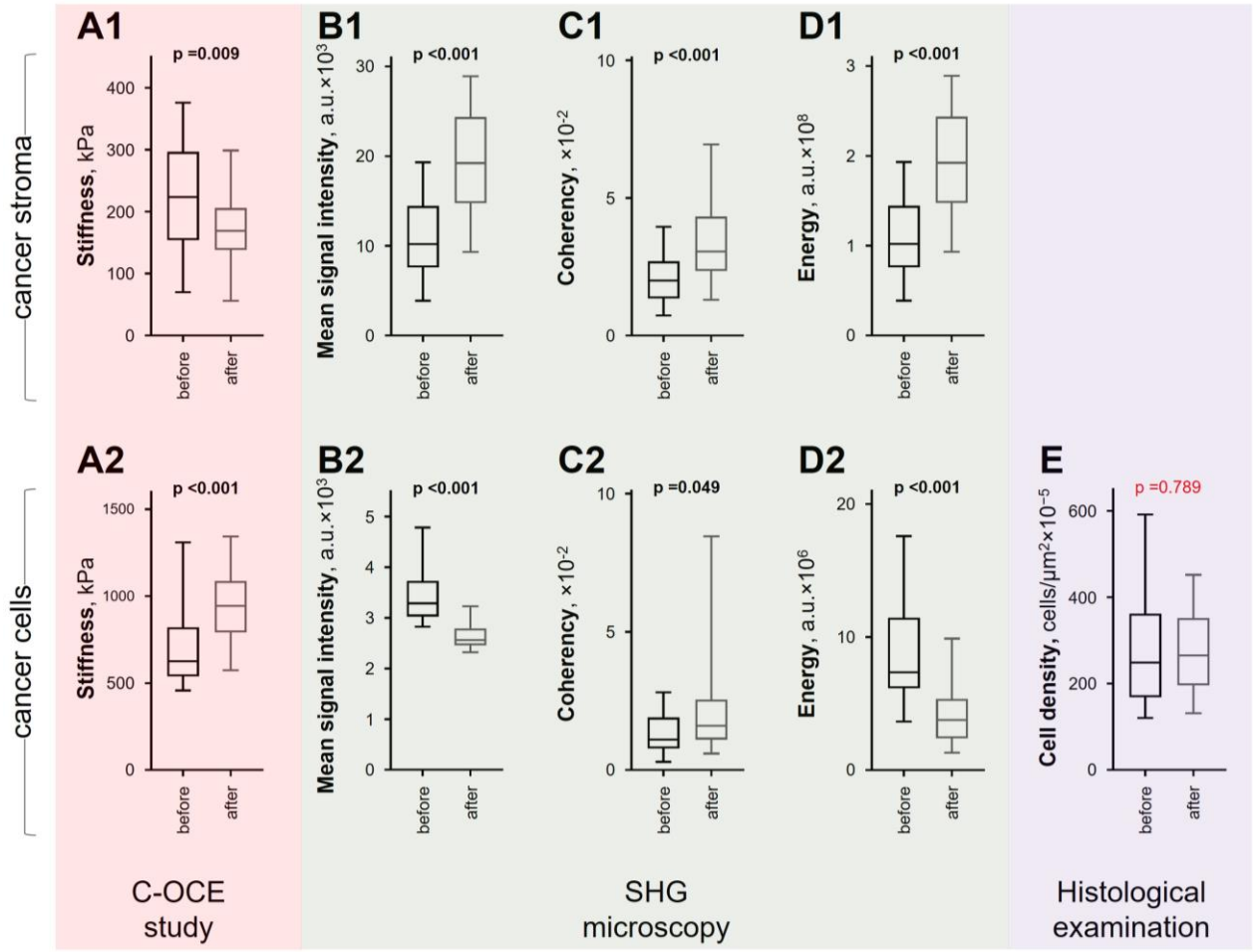

Fig. 3 Quantitative assessment of parameters for cancer stroma areas and cancer cells areas: Stiffness values (A) by C-OCE, Mean signal intensity (B), Coherency (C), and Energy (D) by SHG, and cancer Cell density in standard ROI (E) by histology; for each box plot, the center line represents medians, box plot limits indicate lower/upper quartiles (25th and 75th percentile), whiskers are 5th and 95th percentil; p-values demonstrate statistical significance of the established differences between the corresponding parameters before and after chemotherapy (non-parametric Wilcoxon signed-rank test); a.u. – arbitrary units; the exponential values for arbitrary units are retained in the form given by the ImageJ/OrientationJ software).

3 Results

The obtained histological images (Fig. 2A) from patients before and after the chemotherapy were compared with relevant C-OCE images (Fig. 2B) to determine the stiffness of areas of the cancer stroma and cancer cells. When assessing a full-scale tissue sample, one can note a change in the cellularity of the tumor, which is characteristic of breast cancer tissue after chemotherapy with a pathological partial response [47] – there is a prevalence of fibrosis areas and rare individual clusters of residual cancer cells (Fig. 2A2). When comparing full-scale C-OCE images before and after chemotherapy, there is a decrease in high stiffness values areas (light and dark blue areas in Fig. 2B2) from cancer cells (previously established threshold for detection of cancer cells > 420 kPa [17]) and a predominance of medium and low stiffness values areas (orange and red areas in Fig. 2B2) from cancer stroma after chemotherapy.

In a detailed comparison of histological images of cancer stroma areas and cancer cells areas before and after chemotherapy (Fig. 2C), only thickening of collagen bundles in cancer stroma areas after chemotherapy can be visually noted (Fig. 2C2). There were no visible qualitative features of changes in cancer cells (and in their density positioning relative to each other) or the condition of the collagen fibers after chemotherapy by histology (Fig. 2C4). However, qualitative changes in stiffness before and after chemotherapy were found in C-OCE images: for areas of cancer stroma – a decrease in stiffness was observed (the predominance of orange areas changed to red in Figs. 2D1–D2), and for areas of cancer cells – an increase in stiffness was observed (the predominance of light blue areas changed to dark blue in Figs. 2D3–D4). A detailed visualization of such areas in SHG images shows an expressive change of collagen fibers structure: for areas of cancer stroma – disordered thin collagen fibers are observed before chemotherapy (Fig. 2E1), and an increase in the number of collagen bundles, their orientational ordering and thickening are observed after chemotherapy (Fig. 2E2); within areas of cancer cells randomly oriented isolated collagen fibers are observed

before chemotherapy (Fig. 2E3) and demonstrate almost complete disappearance after chemotherapy (Fig. 2E4).

Then, a quantitative assessment was carried out to determine the significance of differences in the studied parameters before and after chemotherapy. Fig. 3 shows the corresponding results: stiffness values (Fig. 3A) according to C-OCE images, mean SHG-signal intensity (Fig. 3B), parameters of coherency (Fig. 3C) and energy (Fig. 3D) of collagen fibers extracted from SHG images, and the cancer-cell density in a standard ROI (Fig. 3E) extracted from histological images. C-OCE indicated that for *cancer stroma* areas, the stiffness values statistically significantly *decreased* from 224 ± 95 kPa before chemotherapy down to 175 ± 67 kPa after chemotherapy ($p = 0.009$) (Fig. 3A1). However, the analysis of SHG-images of these areas revealed a statistically *significant increase* ($p < 0.001$) in the SHG-based parameters of collagen texture after chemotherapy compared with the pre-chemotherapy values. Namely, mean signal intensity increased from $(11.0 \pm 4.5) \times 10^3$ a.u. to $(19.4 \pm 5.9) \times 10^3$ a.u., coherency increased from $(2.1 \pm 1.0) \times 10^{-2}$ to $(3.5 \pm 1.7) \times 10^{-2}$, and energy increased from $(1.0 \pm 0.5) \times 10^8$ a.u. to $(1.7 \pm 0.6) \times 10^8$ a.u. (see Figs. 3B1–D1). Increase in the mean signal intensity indicates the increase in collagen content in cancer stoma. Increase in the coherency и energy parameters indicate post-chemotherapy increase in orientational ordering accompanied by increase in spatial heterogeneity of the collagen fibers texture.

For *cancer cells* areas, C-OCE, on the contrary to stroma, indicated that stiffness statistically significantly *increased* after chemotherapy from 719 ± 264 kPa to 954 ± 231 kPa ($p < 0.001$) (Fig. 3A2). The SHG analysis of these areas, also in contrast to stroma, revealed a statistically significant post-chemotherapy *decrease* ($p < 0.001$) in the mean signal intensity from $(3.5 \pm 0.6) \times 10^3$ a.u. down to $(2.6 \pm 0.2) \times 10^3$ a.u., as well as in the energy parameter, from $(8.7 \pm 4.1) \times 10^6$ a.u. down to $(4.2 \pm 2.3) \times 10^6$ a.u. (see Figs. 3B2 and 3D2). These results indicate that the content of collagen fibers decreases (the texture visually becomes more rarified). This also led to a decrease in the heterogeneity of the collagen texture reflected in the decrease in the "energy" parameter of the texture. An increase ($p = 0.049$) in the coherency parameter in SHG images of cancer-cell areas after chemotherapy, from $(1.3 \pm 1.0) \times 10^{-2}$ to $(2.7 \pm 3.3) \times 10^{-2}$ (see Fig. 3C2), indicates some increase in the orientational ordering of the collagen fibers residual post therapy.

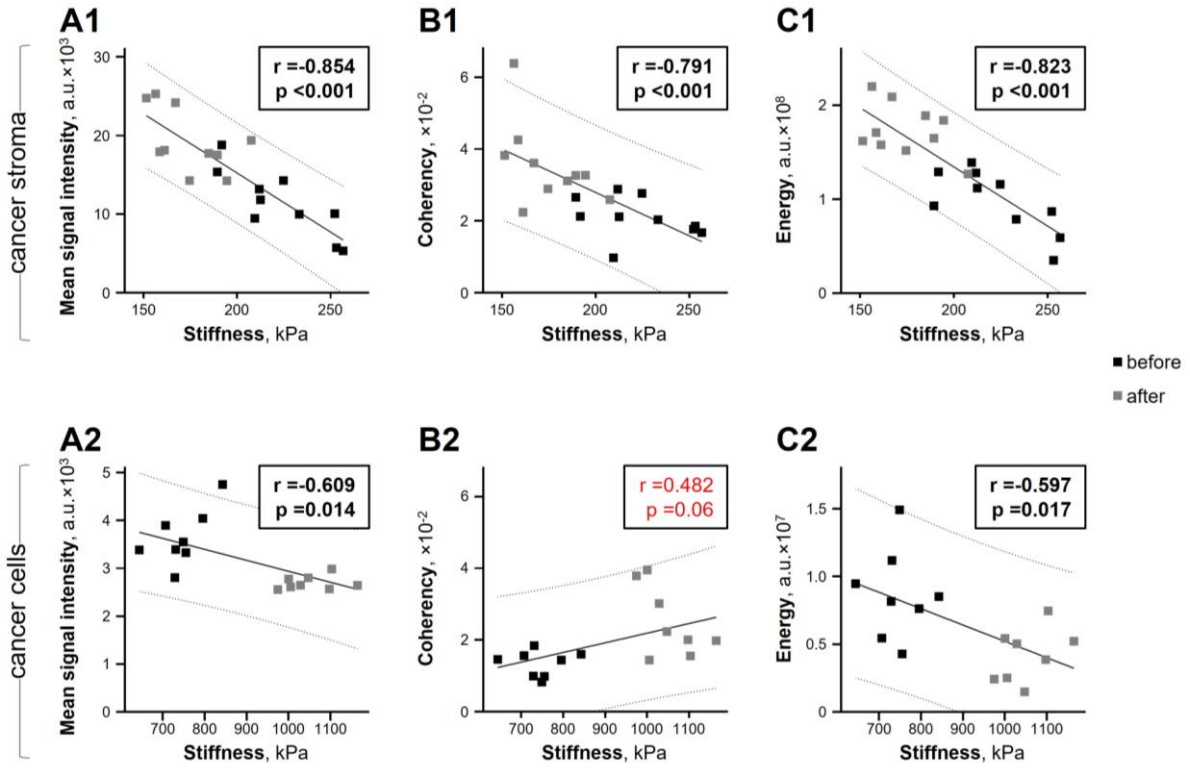

Fig. 4 Relation between stiffness values (according to C-OCE) and values of mean signal intensity, coherency, energy (according to SHG) for areas of cancer stroma (A1–C1) and cancer cells (A2–C2); high inverse significant correlation is demonstrated between stiffness values and mean signal intensity ($r = -0.854$, $p < 0.001$) (A1) / coherency ($r = -0.791$, $p < 0.001$) (B1) / energy ($r = -0.823$, $p < 0.001$) (C1) for cancer stroma areas; lower significant inverse correlation is demonstrated between stiffness values and mean signal intensity ($r = -0.609$, $p = 0.014$) (A2) / energy ($r = -0.597$, $p = 0.017$) (C2) for cancer cells areas; a significant correlation has not been established between stiffness values and coherency ($r = 0.482$, $p = 0.06$) (B2) for cancer cells areas; black squares are values for breast cancer cases before chemotherapy; gray squares are values for breast cancer cases after chemotherapy; the dotted lines show 95% prediction intervals; a.u. – arbitrary units; exponential values for arbitrary units are kept in the form given by the ImageJ/OrientationJ software.

When analyzing the cancer cell density in a standard ROI in histological images (Fig. 3E) before and after chemotherapy (284.9 ± 144.0 cell/$\mu m^2 \times 10^{-5}$ versus 276.8 ± 90.6 cell/$\mu m^2 \times 10^{-5}$), no statistically significant differences were found ($p = 0.789$).

In order to analyze the relation between stiffness values according to C-OCE data and values of mean signal intensity / coherency / energy according to SHG data, or cancer cell density according to histology data the correlation coefficients were calculated separately for areas of cancer stroma (Figs. 4A1, B1, C1) and for cancer cells (Figs. 4A2, B2, C2). There was a high negative (inverse) correlation between the stiffness of cancer stroma areas and their parameters of mean signal intensity ($r = -0.854$, $p < 0.001$), coherency ($r = -0.791$, $p < 0.001$), and energy ($r = -0.823$, $p < 0.001$) (Figs. A1–C1). Also there was an inverse correlation between the stiffness of cancer cells areas and their SHG parameters of mean signal intensity ($r = -0.609$, $p = 0.014$) (Fig. A2), and energy ($r = -0.597$, $p = 0.017$) (Fig. C2). No significant correlation has been established between the stiffness of cancer cells areas and SHG parameter of coherency ($r = 0.482$, $p = 0.06$) (Fig. B2).

4 Discussion

To the best of our knowledge in the reported study for the first time side-by-side high-resolution C-OCE-based characterization of stiffness with SHG-based characterization of collagen texture in patients' breast-cancer tissues before and after chemotherapy. Our earlier study [17] in agreement with other authors [15, 20] already demonstrated the possibility to efficiently characterize various morphological types of breast cancer using C-OCE and even to perform quantitative morphometric analysis of fresh tissue samples using the established differences in stiffness for regions of cancer cells (high stiffness values) and cancer stroma (medium and low stiffness values). Besides, in our recent study related to C-OCE-based evaluation of breast-cancer response to chemotherapy, a certain increase in stiffness of cancer-cell regions post neoadjuvant chemotherapy was revealed [22] in comparison with cancer-cell regions in samples from patients who did not receive chemotherapy before surgery [17]. Furthermore, in the present study elastic properties were studied using needle core biopsy tissue samples (before chemotherapy) and surgery tissue samples (after chemotherapy) taken from the same patients. The obtained results directly confirmed the fact of statistically significant ($p < 0.001$) increase in stiffness of residual cancer-cell regions post chemotherapy (954 ± 231 kPa) in comparison with the stiffness values before chemotherapy (719 ± 264 kPa). It can be noted that the hypothesis that the increase in stiffness of the cancer-cell regions is due to the increase in the density of cancer-cell packing was not confirmed. It was found that the packing density of cancer cells per unit area (counted in histological images over areas $180\ \mu m \times 180\ \mu m$) did not reveal any statistically significantly differences ($p > 0.78$) between the pre-chemotherapy and post-chemotherapy samples: 284.9 ± 144.0 cell/$\mu m^2 \times 10^{-5}$ and 276.8 ± 90.6 cell/$\mu m^2 \times 10^{-5}$, respectively. Penetrating collagen fibers among cancer cells were hardly seen in such regions in histological images. An inverse situation was seen in the regions of cancer stroma, for which the stiffness values statistically significantly decreased post-chemotherapy down to 175 ± 67 kPa from the pre-therapy 224 ± 95 kPa ($p = 0.009$). However, in histological images for these regions, only a certain thickening of collagen bundles was visible. In view of this we tried to obtain a more detailed information about the morphological differences accompanying the stiffness changes in cancer stroma and cancer-cell regions after breast cancer chemotherapy by using SHG microscopy to quantitatively characterize collagen fibers texture.

The importance of studying collagen as the main structural component of breast-tissue stroma is indicated by the known data on the correlation between the density of breast tissue with the risk of breast cancer development [48]. It was also shown that structural features and biomechanical properties of collagenous environment essentially affect the progressive development of cancer, its molecular characteristics and results of therapy [49]. Our previous studies demonstrated the possibility of identification of various morphological subtypes of breast cancer based on SHG-microscopy data on structural/textural features of collagen fibers [28]. In this study the limited amount of samples did not suffice for performing gradation of the revealed textural features of collagen bundles for multiple morpho-molecular subtypes of breast cancer. Nevertheless, the studies 10 cases of breast cancer before and after chemotherapy statistically significantly indicated the fact of therapy-induced variations in the SHG-based parameters of collagen fibers. For the regions of cancer stroma, statistically significant increase in the following SGH-based textural parameters was revealed ($p < 0.001$): mean signal intensity increase from $(11.0 \pm 4.5) \times 10^3$ a. u. to $(19.4 \pm 5.9) \times 10^3$ a. u. after chemotherapy; coherency increased from $(2.1 \pm 1.0) \times 10^{-2}$ to $(3.5 \pm 1.7) \times 10^{-2}$ after chemotherapy; energy increased from $(1.0 \pm 0.5) \times 10^8$ a. u. to $(1.7 \pm 0.6) \times 10^8$ a. u. after chemotherapy. These findings indicate the overall increase in the collagen content accompanied by increase in orientational ordering the collagen bundles and increase in spatial inhomogeneity of the collagen fibers texture after chemotherapy, which is also visually noticeable (Figs. 2E1–E2) and correlates with the results of other authors [50, 51]. Reorganization of collagen bundles and their structuring along a dominant direction may be associated with easier migration of cancer cells along the aligned collagen bundles in cases of weak cancer response to the chemotherapy [52, 53]. In this context, studies [54, 55] can be mentioned, in which differences were found in the SHG-based parameters between cases of pathological complete response of cancer to chemotherapy and cases of partial response. Our plans for future foresee to study a larger amount of cases corresponding to pathological complete and

incomplete responses to chemotherapy for performing side-by-side evaluation of variations in stiffness and SHG-based parameters to reveal differences and determine characteristic values of these parameters for each type of cancer response to the therapy.

For the cancer-cell regions before chemotherapy, in the SHG images thin isolated and randomly directed collagen fibers are fairly well visible (Fig. 2E3), whereas after chemotherapy, collagen fibers among clusters of residual cancer cells visually almost disappear (Fig. 2E4). Statistical analysis of SHG images indicates significant reduction in the following parameters of collagen fibers texture ($p < 0.001$): mean signal intensity – before $(3.5 \pm 0.6) \times 10^3$ a. u and $(2.6 \pm 0.2) \times 10^3$ a. u. after chemotherapy; and energy – before $(8.7 \pm 4.1) \times 10^6$ a. u. and $(4.2 \pm 2.3) \times 10^6$ a. u. after chemotherapy. These variations in the collagen fibers texture parameters well agree with the visually observed reduction in the density of collagen fibers penetrating the cancer cell regions. The observed increase of the coherency parameter in the SGH images $(1.3 \pm 1.0) \times 10^{-2}$ before chemotherapy versus $(2.7 \pm 3.3) \times 10^{-2}$ after it) also well agrees with above-mentioned strong reduction in the density of collagen fibers because residual isolated fibers demonstrate certain "preferential orientation" ($p = 0.049$). Such changes in the texture of breast-cancer collagen fibers after neoadjuvant chemotherapy were also mentioned in study [51]. The observed pathomorphological changes in the breast cancer samples are typical in cases of partial response of tumor to chemotherapy, for which quite typical are clusters of residual cancer cells embedded into overgrown collagenous stroma which substituted the regions of necrotic cancer cells that responded to the chemotherapy [56]. These regions of collagenous stroma prevail over the regions of residual cancer cells survived after chemotherapy, which reduces the overall stiffness of the tumor node detectable by instrumental diagnostic methods [57].

The performed C-OCE study and analysis of the complementary SHG images indicate that the stiffness values of cancer stroma areas demonstrate pronounced negative correlation with the SHG parameters of mean signal intensity ($r = -0.854$, $p < 0.001$), coherency ($r = -0.791$, $p < 0.001$) and energy ($r = -0.823$, $p < 0.001$). The SHG images indicate the increase in the content of collagen fiber, increased orientational ordering (coherency) and increase in the heterogeneity (energy) of the collagen fibers texture. These facts give reasons to assume that it is the change in the structural characteristics of the collagen fibers which give the dominating contribution in the decrease in stiffness of cancer stoma (and overall stiffness reduction of the tumor) after chemotherapy. These conclusions are consistent with the results of our previous C-OCE study [58] of elastic properties of the vaginal wall, in which a high correlation was observed between the wall stiffness and parameters of collagen bundles extracted from quantitative analysis of histological images with Van Gieson staining. It was found that the increase in the vaginal wall stiffness was accompanied by decrease in the coherency (orientational ordering) of collagen bundles, whereas the energy parameter of collagen fibers texture in the histological images increased. Therefore, for the vaginal wall in Ref. [58], the correlation between stiffness and coherency of the collagen fibers texture was also negative like in the present study, whereas for stiffness-energy, the positive sign of correlation in Ref. [58] was opposite to the negative correlation revealed in the present study. In this context it can be pointed out that in Ref. [58] the parameters of collagen bundles texture were estimated using Van-Gieson stained histological images rather that SHG-images used in the present study. Concerning orientation of collagen bundles, these two types of images could give fairly similar results (at least qualitatively), whereas for estimation of texture energy, the results based on stained histological images and SHG-microscopy could differ rather significantly.

For the regions of cancer cells penetrated by collagen fibers, the sign of correlation between stiffness and collagen fibers texture coherency is opposite than for regions of cancer stroma (compare Fig. 4B2 and Fig. 4B1). In contrast, the revealed negative signs of correlation between stiffness and intensity ($r = -0.597$, $p = 0.017$) and between stiffness and collagen fibers texture energy ($r = -0.597$, $p = 0.017$) for cancer-cell regions qualitatively agree with the corresponding correlations found for cancer stroma (see Fig. 4), although the correlation coefficients are somewhat smaller than for stromal regions. The latter fact may be attributed to the stronger contribution of cancer cells themselves to stiffness of cancer-cell regions. In this study we limited ourselves by estimations of densities (concentrations) of the cancer cells before and after chemotherapy putting aside possible structural changes in the individual cancer cells caused by the therapy. Studying of such biomechanical characteristics with a sub-cellular resolution require high-resolution methods such as atomic-force microscopy (AFM) [59]. However, application of this technique for studying intact tissues and, moreover, living tissues is very challenging. Usually, AFM require utilization of either cell-culture samples or tissue slices in the surface layer of which there are very few cells with unperturbed structure [60]. Under such visualization conditions, the influence of mechanical inter-cellular transduction and influence of surrounding cells and extra-cellular matrix may be strongly perturbed [10, 61]. At the same time, it is known (e.g., based on electron-microscopy data [62]) that cell malignization is accompanied by essential disorganization of actin cytoskeleton, which is likely to affect elastic properties of individual cells and may be responsible for the appearance of the so-called higher elasticity peak according to AFM results [59, 63]. However, influence of chemotherapy on the state of cyto-skeleton of residual cancer cell has not yet been studied. Besides, presently there is no sufficient understanding of the contribution of nuclei to the cellular stiffness, although the fact of some increase in the nuclei's sizes

after chemotherapy is known [64]. In view of this only the use of multiparameter analysis of data form various diagnostic techniques may give sufficiently ample understanding of the contributions of various morphological components to the overall stiffness of biological tissues.

5 Conclusion

In this study we performed side-by-side OCE characterization of elasticity collagenous stromal tissue and quantitative characterization of collagen texture using SHG imaging in patients' breast-cancer tissues before and after chemotherapy. The analysis of cancer stromal tissue (i.e. collagen fibers fairly distant from conglomerates of cancer cells) was performed separately from the regions of cancer itself (i.e., clusters of cancer cells penetrated by collagen fibers in the tumor bulk). For the regions of cancer stromal tissue after chemotherapy the performed C-OCE examinations for the first time revealed statistically significant reduction in stiffness ($p = 0.009$). In parallel, the SHG microscopy indicated the statistically significant increase in the amount of collagen bundles accompanied by increase in their coherency and thickening ($p < 0.001$). The revealed high negative correlation ($p < 0.001$) between the stiffness and the SHG-based parameters of collagen texture indicate an important contribution of the collagen organization and collagen-bundle thickening to the reduction of stiffness of the cancer stroma areas after chemotherapy. For the regions of residual cancer cells post chemotherapy, C-OCE for the first time revealed statistically significant opposite trends: increase in stiffness ($p < 0.001$), whereas SHG microscopy indicated statistically significant decrease in the amount of penetrating collagen fibers ($p = 0.014$) and reduction in their thickness ($p = 0.017$). The revealed negative correlation ($p = 0.014$–0.017) between the stiffness of these regions and SHG-based parameters characterizing the amount and uniformity of visualized collagen fibers also indicates the existence of some relationship between the reduction of the collagen-fiber proportion and increase in stiffness of the residual cancer-cell regions after chemotherapy. Further studies will be focused on characterization of post-chemotherapy changes in the cancer cells themselves and clarification of the relationship of these changes with variations in their elastic.

Appendix

This section describes in more detail how the parameters "intensity", "energy" and "coherency" were calculated for the acquired SHG images using the ImageJ / OrientationJ software [44].

Mean signal intensity is a simple first-order moment used to estimate the intensity of the SHG signal, the parameter is calculated over a rectangular processing window by Eq. (1A):

$$< I >= \frac{1}{N^2}\sum_{i=1}^{N}\sum_{j=1}^{N} I(i,j)\,, \qquad (1A)$$

where N is the size of the processing window and $I(i,j)$ is the intensity of a pixel with coordinates (i,j).

The coherency and energy parameters are expressed via spatial derivatives I_x and I_y of the image matrix $I(x,y)$ along the principal directions x and y, respectively, from which a 2×2 symmetric positive matrix J is composed,

$$J = \begin{bmatrix} \langle I_x, I_x \rangle_w & \langle I_x, I_y \rangle_w \\ \langle I_x, I_y \rangle_w & \langle I_y, I_y \rangle_w \end{bmatrix}. \qquad (2A)$$

In Eq. (2A), $<..>_w$ denotes the weighted inner product, which for two quantities is defined as

$$< g,h >_w = \int\int w(x,y)g(x,y)h(x,y)dxdy\,. \qquad (3A)$$

Here, $w(x,y)$ is the Gaussian weighting function that specifies the area of interest. Once the structure tensor in Eq. (2A) is known, the quantities "energy" and "coherency" in the vicinity of each pixel can be calculated [44, 65].

The energy parameter (E) is given by the trace of the tensor matrix:

$$E = Trace(J) = \langle I_x, I_x \rangle_\omega + \langle I_y, I_y \rangle_\omega\,. \qquad (4A)$$

The coherency parameter (C) is defined as the ratio of the difference and the sum of the maximal and minimal eigenvalues λ_{max} and λ_{min} of tensor J,

$$C = \frac{\lambda_{max} - \lambda_{min}}{\lambda_{max} + \lambda_{min}} = \frac{\sqrt{(\langle I_y, I_y \rangle_w - \langle I_x, I_x \rangle_w)^2 + 4\langle I_x, I_y \rangle_w}}{\langle I_x, I_x \rangle_w + \langle I_y, I_y \rangle_w}. \qquad (5A)$$

Coherency is bounded between 0 and 1, with 1 indicating highly oriented structures and 0 indicating isotropic regions.

The OrientationJ software realizes calculation of tensor J defined by Eq. (2A) and then the energy and coherency parameters defined by Eqs. (4A) and (5A).

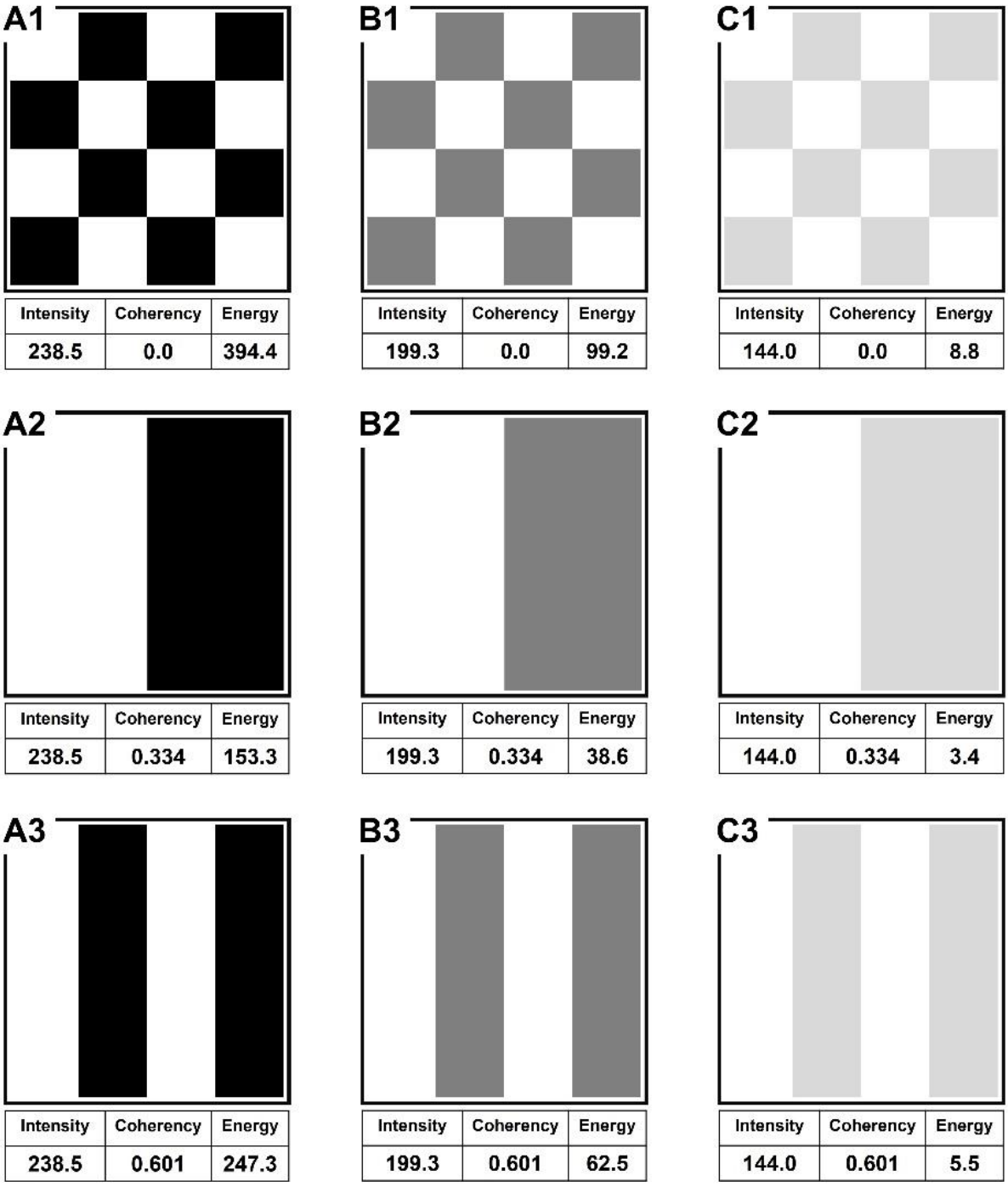

	Intensity	Coherency	Energy
A1	238.5	0.0	394.4
B1	199.3	0.0	99.2
C1	144.0	0.0	8.8
A2	238.5	0.334	153.3
B2	199.3	0.334	38.6
C2	144.0	0.334	3.4
A3	238.5	0.601	247.3
B3	199.3	0.601	62.5
C3	144.0	0.601	5.5

Fig. 1A The test images and the corresponding parameters of mean signal intensity, coherency and energy calculated with the ImageJ/OrientationJ software for each image.

To illustrate the correspondence of these parameters with visually seen image features, we processed a series of simple test images shown in Fig. 1A with the ImageJ/OrientationJ software.

We start from images with a chess-board-like structure, in which dark squares are characterized by various levels of grey color (compare panels A1, B1, C1). The patterns in the upper row have no preferred orientation, so that the coherency parameter is zero, whereas for the invariable pattern geometry, the parameters of intensity and energy monotonically decrease with decreasing contrast of the darker squares.

The 2nd and 3rd rows in Fig. 1A are obtained by reordering the same white and dark squares as in the upper-row images towards more oriented structures with the visually most pronounced pattern orientation in the 3rd row.

The intensity parameter evidently remains insensitive to rearrangement of the squares in each column of Fig. 1A according to the definition given by Eq. (1A). Consequently, the intensity parameter remains invariable

for each column in Fig. 1A (albeit different for different columns).

The energy parameter, for a given grey-color intensity, is maximal for the upper-row images, characterized by the most pronounced spatial heterogeneity and maximal length of boundaries separating white and dark squares, where spatial gradients are localized. Notice that for the same geometrical structure in each row in Fig. 1A, the energy parameter is higher for patterns with higher grey levels.

Finally, the coherency parameter is maximal for the lowest row in Fig. 1A, where the patterns visually demonstrate the most pronounced orientation. Unlike the energy parameter, the coherency parameter is entirely determined by the pattern geometry and is insensitive to the grey level according to the definition given by Eq. (5A). Consequently, the coherency parameter remains invariable for each row in Fig. 1A.

Acknowledgements

The study was funded by the Russian Science Foundation (Grant No. 18-75-10068). The OCT-system adaptation was supported by the contract № 075-15-2022-316 with the Ministry of Science and Higher Education of Russian Federation. The authors thank Maria Karabut and Alexandra Bogomolova (PRMU) for their help in conducting experiments.

Disclosures

The authors declare no conflict of interest.

References

1. H. S. Lahoti, S. D. Jogdand, "Bioimaging: Evolution, Significance, and Deficit," Cureus 14(9), e28923 (2022).
2. R. Leitgeb, F. Placzek, E. Rank, L. Krainz, R. Haindl, Q. Li, M. Liu, M. Andreana, A. Unterhuber, T. Schmoll, and W. Drexler, "Enhanced medical diagnosis for dOCTors: a perspective of optical coherence tomography," Journal of Biomedical Optics 26(10), 100601 (2021).
3. A. H. Kashani, C. L. Chen, J. K. Gahm, F. Zheng, G. M. Richter, P. J. Rosenfeld, Y. Shi, and R. K. Wang, "Optical coherence tomography angiography: A comprehensive review of current methods and clinical applications," Progress in Retinal and Eye Research 60, 66–100 (2017).
4. K. A. Achkasova, A. A. Moiseev, K. S. Yashin, E. B. Kiseleva, E. L. Bederina, M. M. Loginova, I. A. Medyanik, G. V. Gelikonov, E. V. Zagaynova, and N. D. Gladkova, "Nondestructive label-free detection of peritumoral white matter damage using cross-polarization optical coherence tomography," Frontiers in Oncology 13, 1133074 (2023).
5. A. A. Moiseev, M. A. Sirotkina, A. L. Potapov, L. A. Matveev, N. N. Vagapova, I. A. Kuznetsova, and N. D. Gladkova, "Lymph vessels visualization from optical coherence tomography data using depth-resolved attenuation coefficient calculation," Journal of Biophotonics 14(9), e202100055 (2021).
6. H. M. Leung, M. L. Wang, H. Osman, E. Abouei, C. MacAulay, M. Follen, J. A. Gardecki, and G. J. Tearney, "Imaging intracellular motion with dynamic micro-optical coherence tomography," Biomedical Optics Express 11(5), 2768–2778 (2020).
7. S. Wang, K. V. Larin, "Optical coherence elastography for tissue characterization: a review," Journal of Biophotonics 8(4), 279–302 (2015).
8. V. Y. Zaitsev, A. L. Matveyev, L. A. Matveev, A. A. Sovetsky, M. S. Hepburn, A. Mowla, and B. F. Kennedy, "Strain and elasticity imaging in compression optical coherence elastography: The two-decade perspective and recent advances," Journal of Biophotonics 14(2), e202000257 (2021).
9. J. A. Mulligan, G. R. Untracht, S. N. Chandrasekaran, C. N. Brown, and S. G. Adie, "Emerging Approaches for High-Resolution Imaging of Tissue Biomechanics With Optical Coherence Elastography," IEEE Journal of Selected Topics in Quantum Electronics 22(3), 246–265 (2016).
10. B. F. Kennedy, P. Wijesinghe, and D. D. Sampson, "The emergence of optical elastography in biomedicine," Nature Photonics 11(4), 215–221 (2017).
11. A. A. Plekhanov, M. A. Sirotkina, A. A. Sovetsky, E. V. Gubarkova, S. S. Kuznetsov, A. L. Matveyev, L. A. Matveev, E. V. Zagaynova, N. D. Gladkova, and V. Y. Zaitsev, "Histological validation of in vivo assessment of cancer tissue inhomogeneity and automated morphological segmentation enabled by Optical Coherence Elastography," Scientific Reports 10(1), 11781 (2020).
12. M. A. Sirotkina, E. V. Gubarkova, A. A. Plekhanov, A. A. Sovetsky, V. V. Elagin, A. L. Matveyev, L. A. Matveev, S. S. Kuznetsov, E. V. Zagaynova, N. D. Gladkova, and V. Y. Zaitsev, "In vivo assessment of functional and morphological alterations in tumors under treatment using OCT-angiography combined with OCT-elastography," Biomedical Optics Express 11(3), 1365–1382 (2020).
13. P. Wijesinghe, B. F. Kennedy, and D. D. Sampson, "Optical elastography on the microscale," in Tissue Elasticity Imaging, S. K. Alam, B. S. Garra (Eds.), Elsevier, Amsterdam, 185–229 (2020).
14. D. Kashyap, D. Pal, R. Sharma, V. K. Garg, N. Goel, D. Koundal, A. Zaguia, S. Koundal, and A. Belay, "Global Increase in Breast Cancer Incidence: Risk Factors and Preventive Measures," BioMed Research International 2022, 9605439 (2022).

15. B. F. Kennedy, R. A. McLaughlin, K. M. Kennedy, L. Chin, P. Wijesinghe, A. Curatolo, A. Tien, M. Ronald, B. Latham, C. M. Saunders, and D. D. Sampson, "Investigation of Optical Coherence Microelastography as a Method to Visualize Cancers in Human Breast Tissue," Cancer Reseach 75(16), 3236–3245 (2015).
16. E. V. Gubarkova, A. A. Sovetsky, L. A. Matveev, A. L. Matveyev, D. A. Vorontsov, A. A. Plekhanov, S. S. Kuznetsov, S. V. Gamayunov, A. Y. Vorontsov, M. A. Sirotkina, N. D. Gladkova, and V. Y. Zaitsev, "Nonlinear Elasticity Assessment with Optical Coherence Elastography for High-Selectivity Differentiation of Breast Cancer Tissues," Materials 15(9), 3308 (2022).
17. E. V. Gubarkova, A. A. Sovetsky, V. Y. Zaitsev, A. L. Matveyev, D. A. Vorontsov, M. A. Sirotkina, L. A. Matveev, A. A. Plekhanov, N. P. Pavlova, S. S. Kuznetsov, A. Y. Vorontsov, E. V. Zagaynova, and N. D. Gladkova, "OCT-elastography-based optical biopsy for breast cancer delineation and express assessment of morphological/molecular subtypes," Biomedical Optics Express 10(5), 2244–2263 (2019).
18. E. V. Gubarkova, E. B. Kiseleva, M. A. Sirotkina, D. A. Vorontsov, K. A. Achkasova, S. S. Kuznetsov, K. S. Yashin, A. L. Matveyev, A. A. Sovetsky, L. A. Matveev, A. A. Plekhanov, A. Y. Vorontsov, V. Y. Zaitsev, and N. D. Gladkova, "Diagnostic Accuracy of Cross-Polarization OCT and OCT-Elastography for Differentiation of Breast Cancer Subtypes: Comparative Study," Diagnostics 10(12), 994 (2020).
19. D. A. Vorontsov, E. V. Gubarkova, M. A. Sirotkina, A. A. Sovetsky, A. A. Plekhanov, S. S. Kuznetsov, D. A. Davydova, A. Y. Bogomolova, V. Y. Zaitsev, S. V. Gamayunov, A. Y. Vorontsov, V. A. Sobolevskiy, and N. D. Gladkova, "Multimodal Optical Coherence Tomography for Intraoperative Evaluation of Tumor Margins and Surgical Margins in Breast-Conserving Surgery," Sovremennye tehnologii v medicine 14(2), 26–38 (2022).
20. P. Gong, S. L. Chin, W. M. Allen, H. Ballal, J. D. Anstie, L. Chin, H. M. Ismail, R. Zilkens, D. D. Lakhiani, M. McCarthy, Q. Fang, D. Firth, K. Newman, C. Thomas, J. Li, R. W. Sanderson, K. Y. Foo, C. Yeomans, B. F. Dessauvagie, B. Latham, C. M. Saunders, and B. F. Kennedy, "Quantitative Micro-Elastography Enables In Vivo Detection of Residual Cancer in the Surgical Cavity during Breast-Conserving Surgery," Cancer Research 82(21), 4093–4104 (2022).
21. A. Plekhanov, E. Gubarkova, A. Sovetsky, M. Sirotkina, S. Kuznetsov, L. Matveev, D. Vorontsov, A. Matveyev, E. Zagaynova, V. Zaitsev, and N. Gladkova, "Improvement of breast cancer histological examination by means of multimodal OCT," in European Conferences on Biomedical Optics, 20–24 June 2021, Munich, Germany, EW4A.22 (2021).
22. A. A. Plekhanov, E. V. Gubarkova, M. A. Sirotkina, A. A. Sovetsky, D. A. Vorontsov, L. A. Matveev, S. S. Kuznetsov, A. Y. Bogomolova, A. Y. Vorontsov, A. L. Matveyev, S. V. Gamayunov, E. V. Zagaynova, V. Y. Zaitsev, and N. D. Gladkova, "Compression OCT-elastography combined with speckle-contrast analysis as an approach to morphological assessment of breast cancer tissue," Biomedical Optics Express 14(6), 3037–3056 (2023).
23. T. Oskarsson, "Extracellular matrix components in breast cancer progression and metastasis," The Breast 22, S66–S72 (2013).
24. I. Druzhkova, E. Nikonova, N. Ignatova, I. Koryakina, M. Zyuzin, A. Mozherov, D. Kozlov, D. Krylov, D. Kuznetsova, U. Lisitsa, V. Shcheslavskiy, E. A. Shirshin, E. Zagaynova, and M. Shirmanova, "Effect of Collagen Matrix on Doxorubicin Distribution and Cancer Cells' Response to Treatment in 3D Tumor Model," Cancers 14(22), 5487 (2022).
25. P. J. Keely, A. M. Fong, M. M. Zutter, and S. A. Santoro, "Alteration of collagen-dependent adhesion, motility, and morphogenesis by the expression of antisense alpha 2 integrin mRNA in mammary cells," Journal of Cell Science 108(2), 595–607 (1995).
26. D. Chauhan, S. Geetika, S. Kumar, and R. Kumar, "Combined Interaction of Cellular and Extracellular Components Causes Genetic Cascade Activation in Breast Cancer Metastasis," Oncology 100(6), 354–362 (2022).
27. O. Tezcan, A. S. Elshafei, K. Benderski, E. Rama, M. Wagner, D. Moeckel, R. Pola, M. Pechar, T. Etrych, S. von Stillfried, F. Kiessling, R. Weiskirchen, S. Meurer, and T. Lammers, "Effect of Cellular and Microenvironmental Multidrug Resistance on Tumor-Targeted Drug Delivery in Triple-Negative Breast cancer," Journal of Controlled Release 354, 784–793 (2023).
28. E. V. Gubarkova, V. V. Elagin, V. V. Dudenkova, S. S. Kuznetsov, M. M. Karabut, A. L. Potapov, D. A. Vorontsov, A. Y. Vorontsov, M. A. Sirotkina, E. V. Zagaynova, and N. D. Gladkova, "Multiphoton tomography in differentiation of morphological and molecular subtypes of breast cancer: A quantitative analysis," Journal of Biophotonics 14(5), e202000471 (2021).
29. D. Desa, M. Bhanote, R. Hill, J. Majeski, B. Buscaglia, M. D'Aguiar, R. Strawderman, D. Hicks, B. Turner, and E. Brown, "Second-harmonic generation directionality is associated with neoadjuvant chemotherapy response in breast cancer core needle biopsies," Journal of Biomedical Optics 24(8), 086503 (2019).
30. World Medical Association, "Ethical principles for medical research involving human subjects," European Journal of Emergency Medicine: Official Journal of the European Society for Emergency Medicine 8(3), 221–223 (2001).
31. F. Cardoso, S. Kyriakides, S. Ohno, F. Penault-Llorca, P. Poortmans, I. T. Rubio, S. Zackrisson, and E. Senkus, "Early breast cancer: ESMO Clinical Practice Guidelines for diagnosis, treatment and follow-up," Annals of Oncology 30(8), 1194–1220 (2019).

32. A. A. Plekhanov, M. A. Sirotkina, E. V. Gubarkova, E. B. Kiseleva, A. A. Sovetsky, M. M. Karabut, V. E. Zagainov, S. S. Kuznetsov, A. V. Maslennikova, E. V. Zagaynova, V. Y. Zaitsev, and N. D. Gladkova, "Towards targeted colorectal cancer biopsy based on tissue morphology assessment by compression optical coherence elastography," Frontiers in Oncology 13, 1121838 (2023).
33. V. M. Gelikonov, V. N. Romashov, D. V. Shabanov, S. Y. Ksenofontov, D. A. Terpelov, P. A. Shilyagin, G. V. Gelikonov, and I. A. Vitkin, "Cross-Polarization Optical Coherence Tomography with Active Maintenance of the Circular Polarization of a Sounding Wave in a Common Path System," Radiophysics and Quantum Electronics 60, 897–911 (2018).
34. V. Y. Zaitsev, A. L. Matveyev, L. A. Matveev, E. V. Gubarkova, A. A. Sovetsky, M. A. Sirotkina, G. V. Gelikonov, E. V. Zagaynova, N. D. Gladkova, and A. Vitkin, "Practical obstacles and their mitigation strategies in compressional optical coherence elastography of biological tissues," Journal of Innovative Optical Health Sciences 10(06), 1742006 (2017).
35. A. L. Matveyev, L. A. Matveev, A. A. Sovetsky, G. V. Gelikonov, A. A. Moiseev, and V. Y. Zaitsev, "Vector method for strain estimation in phase-sensitive optical coherence elastography," Laser Physics Letters 15(6), 065603 (2018).
36. A. A. Sovetsky, A. L. Matveyev, L. A. Matveev, D. V. Shabanov, and V. Y. Zaitsev, "Manually-operated compressional optical coherence elastography with effective aperiodic averaging: demonstrations for corneal and cartilaginous tissues," Laser Physics Letters 15(8), 085602 (2018).
37. A. A. Sovetsky, A. L. Matveyev, L. A. Matveev, E. V. Gubarkova, A. A. Plekhanov, M. A. Sirotkina, N. D. Gladkova, and V. Y. Zaitsev, "Full-optical method of local stress standardization to exclude nonlinearity-related ambiguity of elasticity estimation in compressional optical coherence elastography," Laser Physics Letters 17, 065601 (2020).
38. A. A. Sovetsky, A. L. Matveyev, L. A. Matveev, G. V. Gelikonov, and V. Y. Zaitsev, "Mapping Large Strains in Phase-Sensitive OCT: Key Role of Supra-Pixel Displacement Tracking in Incremental Strain Evaluation," Journal of Biomedical Photonics & Engineering 8(3), 030304 (2022).
39. E. V. Gubarkova, D. A. Vorontsov, A. A. Sovetsky, E. L. Bederina, M. A. Sirotkina, A. Yu Bogomolova, S. V. Gamayunov, A. Yu Vorontsov, P. V. Krivorotko, V. Y. Zaitsev, and N. D. Gladkova, "Quantification of linear and nonlinear elasticity by compression optical coherence elastography for determining lymph node status in breast cancer," Laser Physics Letters 20(6), 065601 (2023).
40. A. A. Plekhanov, M. A. Sirotkina, V. Y. Zaitsev, E. V. Gubarkova, S. S. Kuznetsov, E. N. Grigoreva, A. A. Sovetsky, L. A. Matveev, A. L. Matveyev, E. V. Zagaynova, and N. D. Gladkova, "Determining morphological structures' stiffness values of tumor tissue by optical coherence elastography," Proceedings of SPIE 11457, 1145707 (2020).
41. L. B. Mostaço-Guidolin, A. C. Ko, F. Wang, B. Xiang, M. Hewko, G. Tian, A. Major, M. Shiomi, and M. G. Sowa, "Collagen morphology and texture analysis: from statistics to classification," Scientific Reports 3(1), 2190 (2013).
42. Z. Nejim, L. Navarro, C. Morin, and P. Badel, "Quantitative analysis of second harmonic generated images of collagen fibers: a review," Research on Biomedical Engineering 39(1), 273–295 (2023).
43. C. B. Raub, V. Suresh, T. Krasieva, J. Lyubovitsky, J. D. Mih, A. J. Putnam, B. J. Tromberg, and S. C. George, "Noninvasive Assessment of Collagen Gel Microstructure and Mechanics Using Multiphoton Microscopy," Biophysical Journal 92(6), 2212–2222 (2007).
44. R. Rezakhaniha, A. Agianniotis, J. T. Schrauwen, A. Griffa, D. Sage, C. V. Bouten, F. N. van de Vosse, M. Unser, and N. Stergiopulos, "Experimental investigation of collagen waviness and orientation in the arterial adventitia using confocal laser scanning microscopy," Biomechanics and Modeling in Mechanobiology 11, 461–473 (2012).
45. J. Schindelin, I. Arganda-Carreras, E. Frise, V. Kaynig, M. Longair, T. Pietzsch, S. Preibisch, C. Rueden, S. Saalfeld, B. Schmid, J. Y. Tinevez, D. J. White, V. Hartenstein, K. Eliceiri, P. Tomancak, and A. Cardona, "Fiji: an open-source platform for biological-image analysis," Nature Methods 9(7), 676–682 (2012).
46. E. Fonck, G. G. Feigl, J. Fasel, D. Sage, M. Unser, D. A. Rüfenacht, and N. Stergiopulos, "Effect of aging on elastin functionality in human cerebral arteries," Stroke 40(7), 2552–2556 (2009).
47. S. C. Hagenaars, S. de Groot, D. Cohen, T. J. A. Dekker, A. Charehbili, E. Meershoek-Klein Kranenbarg, M. Duijm-de Carpentier, H. Pijl, H. Putter, R. Tollenaar, J. R. Kroep, and W. E. Mesker, "Tumor-stroma ratio is associated with Miller-Payne score and pathological response to neoadjuvant chemotherapy in HER2-negative early breast cancer," International Journal of Cancer 149(5), 1181–1188 (2021).
48. N. F. Boyd, Q. Li, O. Melnichouk, E. Huszti, L. J. Martin, A. Gunasekara, G. Mawdsley, M. J. Yaffe, and S. Minkin, "Evidence that breast tissue stiffness is associated with risk of breast cancer," PLoS One 9(7), e100937 (2014).
49. G. J. Yoshida, A. Azuma, Y. Miura, and A. Orimo, "Activated Fibroblast Program Orchestrates Tumor Initiation and Progression; Molecular Mechanisms and the Associated Therapeutic Strategies," International Journal of Molecular Sciences 20(9), 2256 (2019).
50. S. Wu, Y. Huang, Q. Tang, Z. Li, H. Horng, J. Li, Z. Wu, Y. Chen, and H. Li, "Quantitative evaluation of redox ratio and collagen characteristics during breast cancer chemotherapy using two-photon intrinsic imaging," Biomedical Optics Express 9(3), 1375–1388 (2018).
51. L. Li, Z. Han, L. Qiu, D. Kang, Z. Zhan, H. Tu, and J. Chen, "Label-free multiphoton imaging to assess neoadjuvant therapy responses in breast carcinoma," International Journal of Biological Sciences 16(8), 1376–1387 (2020).

52. P. P. Provenzano, K. W. Eliceiri, J. M. Campbell, D. R. Inman, J. G. White, and P. J. Keely, "Collagen reorganization at the tumor-stromal interface facilitates local invasion," BMC Medicine 4(1), 38 (2006).
53. C. D'Alterio, S. Scala, G. Sozzi, L. Roz, and G. Bertolini, "Paradoxical effects of chemotherapy on tumor relapse and metastasis promotion," Seminars in Cancer Biology 60, 351–361 (2020).
54. D. E. Desa, M. Bhanote, R. L. Hill, J. B. Majeski, B. Buscaglia, M. D'Aguiar, R. Strawderman, D. G. Hicks, B. M. Turner, and E. B. Brown, "Second-harmonic generation directionality is associated with neoadjuvant chemotherapy response in breast cancer core needle biopsies," Journal of Biomedical Optics 24(8), 086503 (2019).
55. L. Li, Z. Han, L. Qiu, D. Kang, Z. Zhan, H. Tu, and J. Chen, "Evaluation of breast carcinoma regression after preoperative chemotherapy by label-free multiphoton imaging and image analysis," Journal of Biophotonics 13(1), e201900216 (2020).
56. E. Provenzano, V. Bossuyt, G. Viale, D. Cameron, S. Badve, C. Denkert, G. MacGrogan, F. Penault-Llorca, J. Boughey, G. Curigliano, J. M. Dixon, L. Esserman, G. Fastner, T. Kuehn, F. Peintinger, G. von Minckwitz, J. White, W. Yang, and W. F. Symmans, "Standardization of pathologic evaluation and reporting of postneoadjuvant specimens in clinical trials of breast cancer: recommendations from an international working group," Modern Pathology 28(9), 1185–1201 (2015).
57. Y. Ma, S. Zhang, J. Li, J. Li, Y. Kang, and W. Ren, "Comparison of strain and shear-wave ultrasounic elastography in predicting the pathological response to neoadjuvant chemotherapy in breast cancers," European Radiology 27, 2282–2291 (2017).
58. E. Gubarkova, A. Potapov, D. Krupinova, K. Shatilova, M. Karabut, A. Khlopkov, M. Loginova, A. Sovetsky, V. Zaitsev, S. Radenska-Lopovok, N. Gladkova, G. Grechkanev, and M. Sirotkina, "Compression Optical Coherence Elastography for Assessing Elasticity of the Vaginal Wall under Prolapse after Neodymium Laser Treatment," Photonics 10(1), 6 (2023).
59. M. Plodinec, M. Loparic, C. A. Monnier, E. C. Obermann, R. Zanetti-Dallenbach, P. Oertle, J. T. Hyotyla, U. Aebi, M. Bentires-Alj, R. Y. H. Lim, and C.-A. Schoenenberger, "The nanomechanical signature of breast cancer," Nature Nanotechnology 7(11), 757–765 (2012).
60. F. Xia, K. Youcef-Toumi, "Review: Advanced Atomic Force Microscopy Modes for Biomedical Research," Biosensors 12(12), 1116 (2022).
61. G. Y. H. Lee, C. T. Lim, "Biomechanics approaches to studying human diseases," Trends in Biotechnology 25(3), 111–118 (2007).
62. S. Havaki, M. Kouloukoussa, K. Amawi, Y. Drosos, L. D. Arvanitis, N. Goutas, D. Vlachodimitropoulos, S. D. Vassilaros, E. Z. Katsantoni, I. Voloudakis-Baltatzis, V. Aleporou-Marinou, C. Kittas, and E. Marinos, "Altered expression pattern of integrin alphavbeta3 correlates with actin cytoskeleton in primary cultures of human breast cancer," Cancer Cell International 7, 16 (2007).
63. A. Stylianou, S. V. Kontomaris, C. Grant, and E. Alexandratou, "Atomic Force Microscopy on Biological Materials Related to Pathological Conditions," Scanning 2019, 8452851 (2019).
64. Z. Han, L. Li, D. Kang, Z. Zhan, H. Tu, C. Wang, and J. Chen, "Label-free detection of residual breast cancer after neoadjuvant chemotherapy using biomedical multiphoton microscopy," Lasers in Medical Science 34, 1595–1601 (2019).
65. B. Jähne(Ed.), Spatio-Temporal Image Processing: Theory and Scientific Applications, Lecture Notes in Computer Science No. 751, Springer-Verlag (1993).